PL-TR-97-2021

SMALL ON-BOARD ENVIRONMENTAL DIAGNOSTIC SENSORS PACKAGE (SOBEDS)

Bronislaw K. Dichter
Marilyn R. Oberhardt
John O. McGarity

AMPTEK, INC.
6 De Angelo Drive
Bedford, MA 01730-2204

7 February 1997
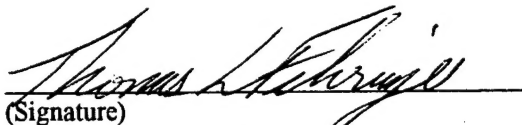
Scientific Report No. 1

19970414 101

PHILLIPS LABORATORY
Directorate of Geophysics
AIR FORCE MATERIEL COMMAND
HANSCOM AFB, MA 01731-3010

DTIC QUALITY INSPECTED 8

This Scientific Report #1 has been reviewed and is approved for publication.
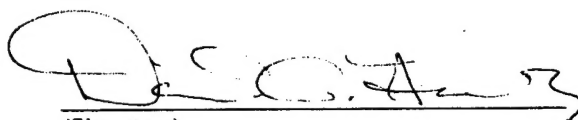

(Signature)
Thomas L. Fehringer, Lt, USAF
Contract Manager

(Signature)
E. Gary Mullen
Branch Chief

(Signature)
David Hardy
Division Director

This report has been reviewed by the ESC Public Affairs Office (PA) and is releasable to the National Technical Information Service (NTIS).

Qualified requestors may obtain additional copies from the Defense Technical Information Center (DTIC). All others should apply to the National Technical Information Service (NTIS).

If your address has changed, if you wish to be removed from the mailing list, or if the addressee is no longer employed by your organization, please notify PL/IM, 29 Randolph Road, Hanscom AFB, MA 01731-3010. This will assist us in maintaining a current mailing list.

Do not return copies of this report unless contractual obligations or notices on a specific document require that it be returned.

REPORT DOCUMENTATION PAGE

Public reporting burden for this collection of information is estimated to average 1 hour per response, including the time for reviewing instructions, searching existing data sources, gathering and maintaining the data needed, and completing and reviewing the collection of information. Send comments regarding this burden estimate or any other aspect of this collection of information, including suggestions for reducing this burden, to Washington Headquarters Services, Directorate for Information Operations and Reports, 1215 Jefferson Davis Highway, Suite 1204, Arlington, VA 22202-4302, and to the Office of Management and Budget, Paperwork Reduction Project (0704-0188), Washington, DC 20503.

1. AGENCY USE ONLY *(Leave blank)*	2. REPORT DATE	3. REPORT TYPE AND DATES COVERED
	07 Feb 1997	Scientific No. 1

4. TITLE AND SUBTITLE

Small On-Board Environmental Diagnostics Sensors Package (SOBEDS)

5. FUNDING NUMBERS

PE 63410F
PR 2822   TA GC   WU AM

Contract F19628-95-C-0227

6. AUTHOR(S)
Bronislaw K. Dichter
Marilyn R. Oberhardt
John O. McGarity

7. PERFORMING ORGANIZATION NAME(S) AND ADDRESS(ES)

AMPTEK, Inc.
6 De Angelo Drive
Bedford, MA 01730

8. PERFORMING ORGANIZATION REPORT NUMBER

9. SPONSORING/MONITORING AGENCY NAME(S) AND ADDRESS(ES)
Phillips Laboratory
29 Randolph Road
Hanscom AFB, MA 01731-3010

Contract Manager: Lt. Tom Fehringer / GPSP

10. SPONSORING/MONITORING AGENCY REPORT NUMBER

PL-TR-97-2021

11. SUPPLEMENTARY NOTES

12a. DISTRIBUTION AVAILABILITY STATEMENT

Approved for public release;
distribution unlimited.

12b. DISTRIBUTION CODE

13. ABSTRACT *(Maximum 200 words)*

The Small On-Board Environmental Diagnostic Sensors Package (SOBEDS) is a suite of spacecraft instruments designed to measure ionizing radiation in the near-Earth space environment. The purpose of data gathered by the SOBEDS instrument is to improve the understanding of the Earth's radiation belts and the effect of ionizing radiation on Air Force space systems. Amptek, Inc. is building three of the SOBEDS instruments: HEP, LEP and DOS. The HEP instrument will measure the differential energy spectrum of protons with energies between 15 and 300 MeV, LEP will measure the differential energy spectra of electrons (0.1 < E < 1 MeV) and protons (1 < E < 15 Mev) and DOS will measure the radiation doses received by electronic components behind four different amounts of shielding.

14. SUBJECT TERMS
Spacecraft Radiation Measurement, Electrons, Protons, Dosimetry

15. NUMBER OF PAGES
28

16. PRICE CODE

17. SECURITY CLASSIFICATION OF REPORT	18. SECURITY CLASSIFICATION OF THIS PAGE	19. SECURITY CLASSIFICATION OF ABSTRACT	20. LIMITATION OF ABSTRACT
Unclassified	Unclassified	Unclassified	SAR

TABLE OF CONTENTS

TABLE OF FIGURES

TABLE OF TABLES

1. INTRODUCTION

This report contains the summary of the scientific and engineering work performed as part of the development of the High Energy Proton (HEP) and Low Energy Particle (LEP) instruments. HEP and LEP are a part of the SOBEDS suite of instruments being developed by Amptek, Inc. under the present contract (F19628-95-C-0227). The purpose of the HEP instrument is to detect incident high energy protons ($15 \leq E \leq 300$ MeV) and measure their energy spectrum. The LEP instrument is intended to measure the differential energy spectra of electrons ($0.1 < E < 1$ MeV) and protons ($1 < E < 15$ MeV).

The primary technical effort during the first year of the SOBEDS contract has been devoted to the design of the HEP sensor head. The key issue in this effort is the choice of scintillator material to be used as the primary proton detector and the size and arrangement of the various sensor head detectors. Section 2 contains the summary of the extensive experimental work carried out to determine the proper choice of HEP scintillator material. The baseline HEP sensor head geometry, as well as its expected performance, is described in Section 3. The baseline design for the LEP sensor is described in Section 4. A summary of the work and concluding remarks are contained in Section 5.

1

2. SCINTILLATOR RESEARCH

2.1. Materials and their Physical Properties

The choice of scintillator material to be used as the primary HEP detector is critical to the proper performance of the instrument. HEP is to measure the differential energy spectrum of in-aperture incident protons with energies between 15 and 300 MeV and the measurement is to be accurate in all parts of the Earth's magnetosphere, including the inner radiation belt. In order to achieve this goal the HEP scintillator must meet three requirements: 1) **high density and stopping power**, 2) **high light output**, and 3) **short light pulse decay time**.

The first requirement (high density) is necessary because dense scintillator material with a high stopping power can be used to make a small detector. This, in turn, has two benefits: 1) the decreased volume of shielding around the detector will result in a smaller mass of the instrument and 2) the smaller sensitive detector volume will decrease the background counting rate while the instrument is in the inner radiation belt. The second requirement (high light output) is necessary to achieve good resolution in the measurement of energy deposited in the scintillator by incident protons. The third requirement (short decay time) is important due to the large event rate in the scintillator in the inner radiation belt.

2.2. Testing and Experimental Work

We have evaluated a number of scintillator materials for use in HEP (see Table 1). Of the materials listed in Table 1, we have obtained all but the LSO. The scintillators are in "flight instrument" size: 2.0 cm diameter and 2.0 cm long. LSO is not currently commercially available but is expected to come on the market in the first half of 1997.

We have conducted extensive testing with γ-ray sources and proton beams in order to determine the proton stopping power, energy resolution and temperature dependence of the light output of the scintillators. Proton stopping power measurements are not yet complete and a final series of proton beam tests is planned for January and March of 1997. We have also undertaken a program of radiation hardness measurements, to be completed in early 1997.

At this time, GSO and LuAP are the leading candidates for HEP scintillators. Both materials have high total light output and excellent stability with variation in temperature. LuAP is denser than GSO and has a larger stopping power than GSO, but GSO has better energy resolution. However, LuAP is new material, still in the development stage, and significant improvement in its performance is possible.

2

Table 1. Listing of physical properties of studied scintillators.

Property	LuAP (LuAlO$_3$)	GSO (Gd$_2$SiO$_5$)	PWO (PbWO$_4$)	LSO (Lu$_2$SiO$_5$)	BGO (Bi$_4$Ge$_3$O$_{12}$)
Density (g/cm^3)	8.4	6.7	8.3	7.4	7.1
Light Output (phot./MeV)	10,900±1,100	7,900±800	100±11	27,000±2,700	8,060±120
Availability	R&D	Product	R&D	R&D	Product
Rad. Hard. (rads)	Not Reported	Protons: 10^7 γ's: 10^9	10^6	Not Reported	10^5-10^6
Resolution (@ 662keV)	9%	11%	Not Reported	13%	11%
Background (cnts/sec-cm^3)	320	None	None	310	None
Hygroscopic	No	No	No	No	No
Light Output: T dependence	Slight	Slight	Not Reported	Not Reported	Strong
Timing: T dependence	Not Reported	Not Reported	Not Reported	Not Reported	Strong

3. BASELINE HEP INSTRUMENT DESIGN

We have developed a baseline design for the HEP instrument. The purpose of this design is to allow both theoretical analysis of the HEP on-orbit performance and experimental tests of key features of HEP operation. Accordingly, we are in the process of building a HEP engineering model, based on the baseline design, for testing with accelerator proton beams. The results of the theoretical and experimental work with the engineering unit will be used to modify the baseline design into the final, flight, HEP configuration.

3.1. Mechanical Configuration

The overall mechanical design concept of the HEP sensor consists of a cylindrical sensor head mounted either directly, or next to, an electronics enclosure, a 4" x 4" x 2-3" Al box. In the final HEP design the location and form factor of the electronics enclosure may be different, although the total volume should stay close to 40 in³. The sensor head will consist of the detector assembly and Cu shielding, in the form of a cylinder, a front collimator and a rear plug. The 0.5 cm thick Cu shielding cylinder, with openings for the photomultipliers (PMT's) will surround the detector assembly. The cylinder will shield the detectors from protons with energies up to 60 MeV protons. The front collimator and rear plug are also made of copper and have a thickness of 1.3 cm (range of 100 MeV protons). The front collimator will have an aperture of 0.25 cm² in area with an opening half-angle of 7°.

A scale drawn sketch of the HEP detectors is shown in Figure 1. The opening half angle, θ, is 7°. The sizes of the various detectors are as follows:

- D1: 700 μm thick, 0.25 cm² area PIPS detector
- D2: 700 μm thick, 0.25 cm² area PIPS detector
- S1: LuAP or GSO scintillator cylinder, 1.5 cm in diameter, 2 cm long
- D3: 700 μm thick, 1.50 cm² area PIPS detector
- S2: LuAP or GSO scintillator cylinder, 2 cm in diameter, 2 cm long
- D4: 700 μm thick, 3.00 cm² area PIPS detector
- S3: Fast Plastic scintillator hollow cylinder, ID = 1.9 cm, OD = 2.5 cm

Notes on Figure 1:

1) PMT's which view the S1 and S2 scintillators are not shown.

2) The S3 scintillator is not a complete cylinder because it must allow the light guides that connect S1 with the PMT to pass through it. S3 will be viewed by 1 or 2 photodiodes or avalanche photodiodes.

3) Cu shielding on one side of the figure has been omitted to show the dimension lines.

4) The actual collimator will have an opening feathered to allow for a 7° opening half-angle and 1.2 mm Al degrader plug which will stop protons with energies below 15 MeV.

All dimensions in cm

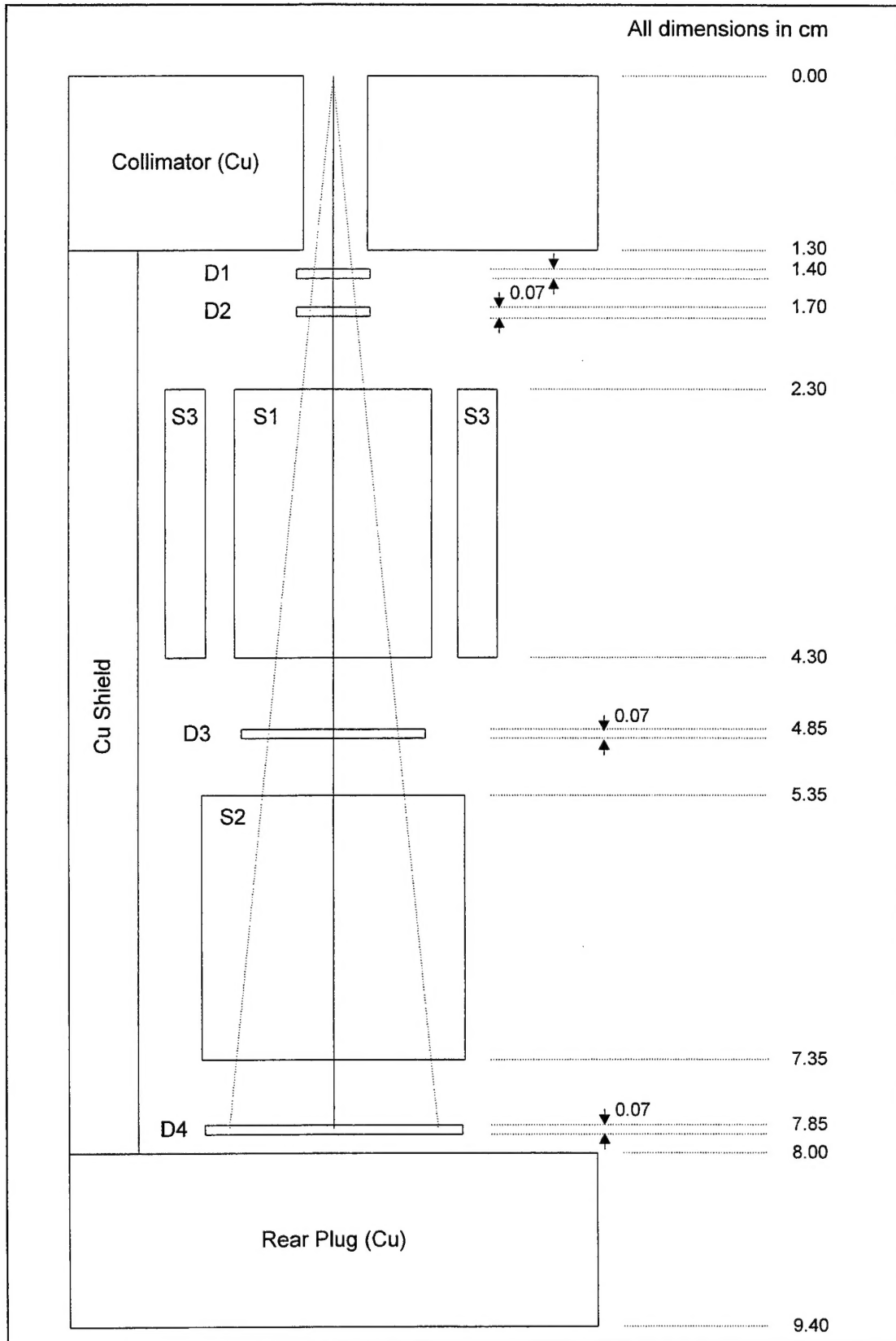|	
Collimator (Cu)	0.00
	1.30
D1	1.40
0.07	
D2	1.70
	2.30
S3 S1 S3	
	4.30
D3 0.07	4.85
	5.35
S2	
	7.35
D4 0.07	7.85
	8.00
Cu Shield	
Rear Plug (Cu)	
	9.40

Figure 1. Sketch of the HEP detector configuration.

The approximate mass of the instrument may be computed from the following:

A) Sensor Head

A.1)   Cu Cylinder: ID $= 3$ cm, OD $= 4$ cm, length $= 6.5$ cm, density $= 8.9$ g/cm^3
$$V_{Cu} = 6.5*[\pi(2.0)^2 - \pi(1.5)^2] \cong 36 \text{ cm}^3$$
$$M_{Cu} = 36 \text{ cm}^3 * 8.9 \text{ g/cm}^3 \cong 320 \text{ g}$$

A.2)   Cu collimator and rear plug: dia. $= 4$ cm, length $= 1.3$ cm, density $= 8.9$ g/cm^3
$$V_W = 2*\pi(2.0)^2 * 1.3 \cong 32.7 \text{ cm}^3$$
$$M_W = 32.7 \text{ cm}^3 * 8.9 \text{ g/cm}^3 \cong 290 \text{ g}$$

A.3)   S1 and S2 scint.: length $= 2$ cm, dia. $= 0.5$ and 1.0 cm, density $= 8.3$ g/cm^3
$$V_{S12} = 2.0*[\pi(1.0)^2 + \pi(0.5)^2] \cong 8 \text{ cm}^3$$
$$M_{S12} = 8 \text{ cm}^3 * 8.3 \text{ g/cm}^3 \cong 65 \text{ g}$$

A.4)   PMT's (Thorn 9112 with divider chain)
$$M_{PMT} = 2 * 70 \text{ g} = 140 \text{ g}$$

A.5)   Misc: D1, D2, D3, D4, S3 + mounting hardware
$$M_{Misc} = 100 \text{ g}$$

B) Electronics enclosure

The enclosure is similar in size but slightly smaller than the CEASE instrument. Total mass should be somewhat smaller than CEASE.

$$M_{Ele} = 900 \text{ g.}$$

The total mass of the HEP baseline design, M_{HEP}, will be

$$M_{HEP} = M_{Cu} + M_W + M_{S12} + M_{PMT} + M_{Misc} + M_{Ele}$$
$$= (320 + 290 + 65 + 140 + 100 + 900) \text{ g}$$
$$= 1.8 \text{ kg} = 4.0 \text{ lb.}$$

3.2. Expected Performance

The HEP instrument will identify incident protons and determine their energy by the pattern of detectors hit by the incident particle and the energy deposited in the detectors, primarily in the S1 and S2 scintillators. In-aperture proton events will be classified into four general types:

Type A: proton traverses D1, D2 and stops in S1,
Type B: proton traverses D1, D2, S1, D3 and stops in S2,
Type C: proton traverses D1, D2, S1, D3, S2 and D4.
Type D: same as Type C but incident proton energy > 300 MeV.

In addition to these four types of events there can be many other types caused by out-of-aperture protons penetrating the HEP shielding.

The various in-aperture event types are caused by protons with different kinetic energies. The energy losses of protons in the HEP solid state detectors and the S1 and S2 scintillators are shown in Figure 2 and Figure 3. Protons with energies above the degrader threshold of 15 MeV and below 120 MeV will stop in S1 and produce Type A events. Type B events are caused by protons with energies above the Type A maximum of 120 MeV and below 175 MeV. Finally, Type C events are due to protons with energies above 175 MeV. A list of energy deposition patterns for in-aperture events is shown in Table 2. Energy losses for event Type C are for a maximum proton energy of 300 MeV. Higher incident energies (Type D events) will produce smaller energy depositions (S1 and S2 < 40 MeV). Note that both front and rear entry protons will be detected as Type C and D events.
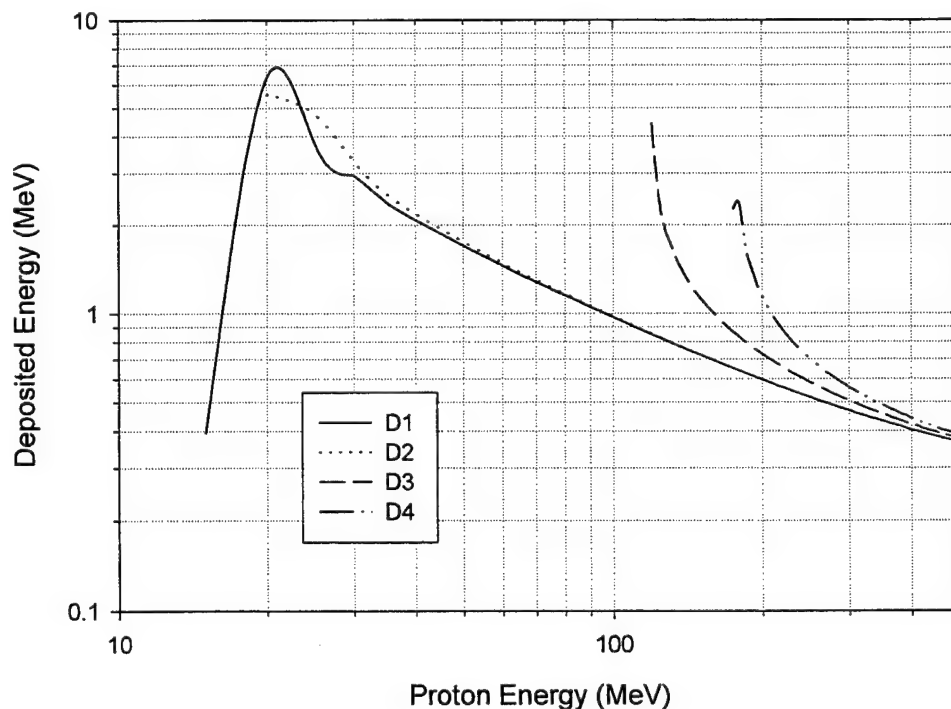

Figure 2. Proton energy loss in HEP solid state detectors (front entry).
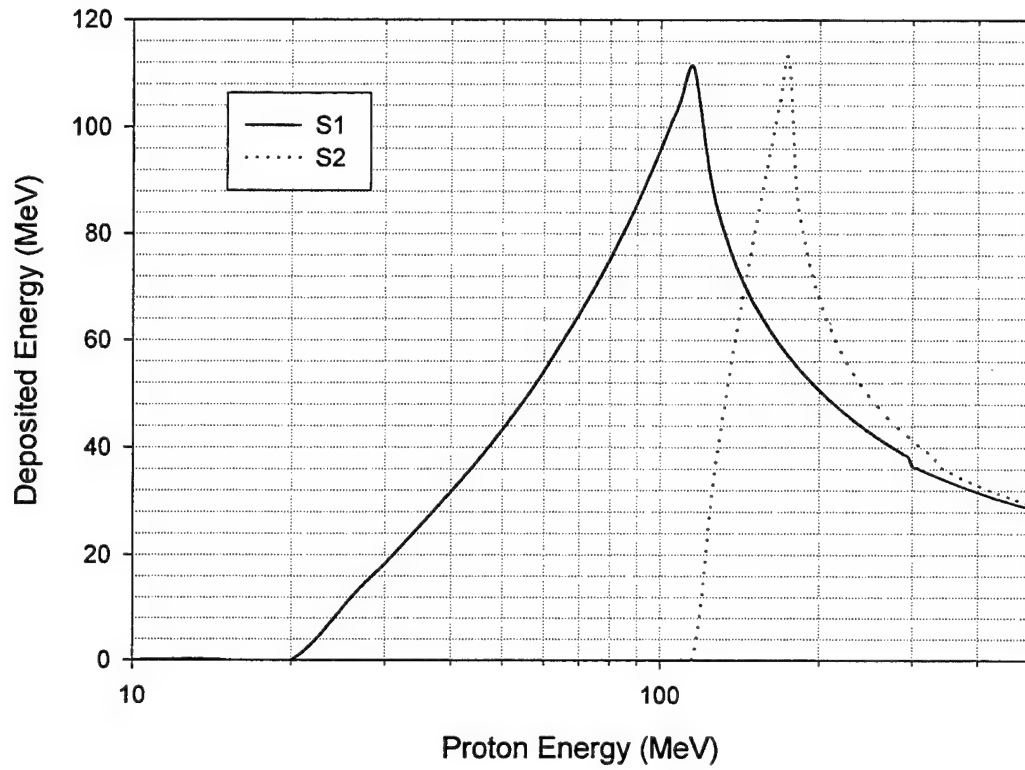
Figure 3. Proton energy loss in HEP S1 and S2 LuAP scintillators (front entry).

Table 2. Listing of proton energy losses (Δ) in HEP detectors.

Event Type	Energy Loss (Δ) in MeV					Total Energy
	D1&D2	D3	D4	S1	S2	
A	0.8<Δ	0	0	Δ<120	0	S1
B	0.6<Δ<0.8	0.8<Δ	0	56<Δ<120	Δ<120	S1+S2
C (Front)	0.5<Δ<0.6	0.5<Δ<0.8	0.5<Δ	36<Δ<56	40<Δ<120	See Text
C (Back)	0.5<Δ<0.6	0.5<Δ<0.8	0.5<Δ	40<Δ<120	36<Δ<56	See Text
D	0.5<Δ	0.5<Δ	0.5<Δ	Δ < 40	Δ < 40	See Text

8

Note that there are several pulse height checks that can be made to help discriminate against bad events. For example, for a good Type B event if S1 > S2 then S1+S2 < 145 MeV and if S2 > S1 then S1+S2 > 145 MeV. Similarly, for a good front entry Type C event, the S1 pulse height must lie between 30 and 60 MeV.

The most difficult HEP measurement is that of the incident proton energy for a Type C event (175 < E < 300 MeV). In this case, the proton punches through all the HEP detectors and does not deposit its full energy in the instrument. The incident energy must be reconstructed from the pattern of energy deposition in S1 and S2. The most straightforward way of making this measurement is to derive it from the pulse height difference S2-S1 for a valid Type C event. The pulse height difference (S2 - S1) as a function of incident proton energy for 200 to 300 MeV front entry protons is shown in Figure 4. The pulse height difference for rear entry protons is the same in magnitude but opposite in sign.

The spread (FWHM) in pulse height distribution is between 5 and 10% of the peak energy for LuAP. This corresponds to 2-4 MeV at the high energy (300 MeV) end and 3-6 MeV at the low energy (200 MeV) end. Thus, it should be possible to subdivide the 200 to 300 MeV energy range into two bins 200-240 MeV and 240-300 MeV. If the S1 and S2 energy resolution is close to, or better than, 5%, three energy bins may be possible.
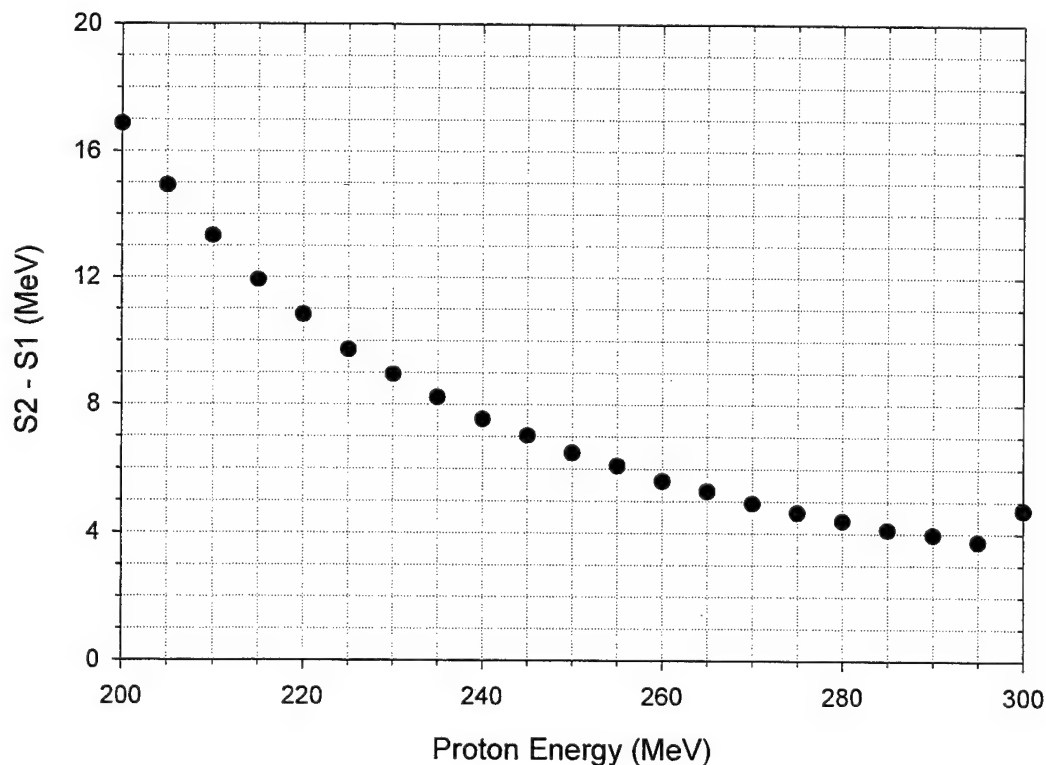

Figure 4. S1-S2 pulse height difference for front entry protons.

The primary high energy proton population is in the inner radiation belt and the HEP instrument must function properly in that environment. The most important aspect of the instrument's operation is that the true energy spectrum of incident protons be accurately reconstructed from HEP data. This can be accomplished by a combination of two techniques: 1) minimizing the possibility of misidentifying the energy of an incident proton and 2) by collecting sufficient "background" data to allow the effects of misidentified particles to be subtracted out from the measured HEP spectra.

The proton fluxes used in this analysis of HEP performance were obtained from the AP8 model. The maximum values of inner belt integral fluxes as a function of threshold energy (regardless of altitude) are listed in

Table 3. If the incident flux is isotropic then the omni-directional flux, F(E), is simply related to the unidirectional flux, f(E) by

$$f(E) = \frac{F(E)}{4\pi} \tag{1}$$

Equation (1) gives a good approximation of f(E) in the equatorial regions. At mid-latitudes the factor in the denominator becomes 3π and near the mirror points the factor is approximately 2π.

Table 3. Maxium proton fluxes in the inner belt (AP8).

Energy (MeV)	Integral Flux p/cm²-sec (x 10³)
5	1,610
10	343
20	63.9
40	29.9
50	25.8
60	22.9
80	18.3
100	14.7
150	8.6
200	5.0
250	3.1
300	1.9

The in-aperture count rate, CR is given by

$$CR\ (E)\ =\ GF \cdot f\ (E)\tag{2}$$

where GF is the geometric factor of the instrument. GF is computed from

$$GF\ =\ 2\pi \int_0^{\theta_m} A(\theta)\sin(\theta)\,d\theta\ =\ \pi\,A_o\,[\,1-\cos^2(\theta_m)\,]\tag{3}$$

where $A(\theta)$ is the, angle dependent, effective area of the aperture, A_o is the total area of the aperture, and θ_m is the maximum angle of travel which allows a particle to reach the aperture. The HEP design under analysis has $A_o = 0.25$ cm^2 and $\theta_m = 7°$, hence GF $= 11.7$ x 10^{-3} cm^2-sr.

Type A Event Counting Rate:

$$\begin{aligned}CR_A\ &=\ GF * [f\ (E > 20\ MeV) - f\ (E > 120\ MeV)\\ &= (11.7\ x\ 10^{-3}\ cm^2\text{-sr})\ (\ (63.9\text{-}11.6)\ x\ 10^3\ p\text{-}cm^{-2}\text{-}sec^{-1})\ /\ (4\pi\ sr)\\ &= 49\ sec^{-1}\end{aligned}$$

Type B Event Counting Rate:

$$\begin{aligned}CR_B\ &=\ GF * [f\ (E > 120\ MeV) - f\ (E > 175\ MeV)\\ &= (11.7\ x\ 10^{-3}\ cm^2\text{-sr})\ (\ (11.6\text{-}6.8)\ x\ 10^3\ p\text{-}cm^{-2}\text{-}sec^{-1})\ /\ (4\pi\ sr)\\ &= 4.5\ sec^{-1}\end{aligned}$$

Type C Event Counting Rate:

$$\begin{aligned}CR_C\ &=\ GF * [f\ (E > 175\ MeV) - f\ (E > 300\ MeV)\\ &= 2\ (11.7\ x\ 10^{-3}\ cm^2\text{-sr})\ (\ (6.8\text{-}1.9)\ x\ 10^3\ p\text{-}cm^{-2}\text{-}sec^{-1})\ /\ (4\pi\ sr)\\ &= 9.1\ sec^{-1}\end{aligned}$$

Type D Event (E > 300 MeV) Counting Rate:

$$\begin{aligned}CR_D\ &=\ GF * [f\ (E > 300\ MeV)\\ &= 2\ (11.7\ x\ 10^{-3}\ cm^2\text{-sr})\ (\ 1.9\ x\ 10^3\ p\text{-}cm^{-2}\text{-}sec^{-1})\ /\ (4\pi\ sr)\\ &= 3.5\ sec^{-1}\end{aligned}$$

Total Counting Rate:

$$CR_T\ =\ CR_A + CR_B + CR_C + CR_D =\ 66.1\ sec^{-1}$$

The factor of 2 for the C and D type events is due to the fact that both in-aperture and rear entry (180° from the aperture normal) high energy particles will produce valid events.

3.3. Background Counting Rates

The singles counting rates of the HEP detectors are the critical parameter in determining the performance of the instrument. These rates, together with the coincidence resolving time, determine the rate of false event identification, which must be kept well below the true, in-aperture, event rate. Since the singles counting rates depend only on the detector geometry and the incident flux, they determine the required coincidence resolving time.

3.3.1. Solid State Detectors (D1, D2, D3 and D4)

The geometric factor of a circular disk for particles incident from the hemisphere on one side of the disk is

$$GF = 2\pi \int_0^{\pi/2} A_0 \cos(\theta) \sin(\theta) \, d\theta = \pi A_0 \tag{4}$$

where A_0 is the disk area. Of course, the disk has a second, equal geometric factor for particles incident from the other hemisphere.

D1 and D2 Detectors:

D1 and D2 are shielded on one side by the front collimator ($E_{th} = 100$ MeV) and on the back side by the S1 scintillator and the side Cu shielding. The back side shielding is thick enough to stop 100 MeV protons. The detectors are both 0.25 cm^2 in area.

$$CR \cong 2\pi A_0 \, f(E{>}100 \text{ MeV}) = 2\pi \, (0.25 \text{ cm}^2) \, (14.7 \times 10^3 \text{ p-cm}^{-2}\text{-sec}^{-1}) / (4\pi \text{ sr})$$

$$= 1,840 \text{ sec}^{-1}$$

The above rate is for penetrating protons (E > 100 MeV) only. The D1 singles rate is further increased by in-aperture protons which penetrate the degrader (15 MeV)

$$CR \cong GF * f(E{>}15 \text{ MeV}) = (11.7 \times 10^{-3} \text{ cm}^2\text{-sr}) \, (200 \times 10^3 \text{ p-cm}^{-2}\text{-sec}^{-1}) / (4\pi \text{ sr})$$

$$= 186 \text{ sec}^{-1}$$

Thus the D1 and D2 singles rates, CR_{D12}, are about 2,000 sec^{-1}.

D3 Detector:

D3 is shielded on each side by the large scintillators (S1 and S2) so that the minimum proton threshold energy is at least 100 MeV. The detector area is 1.5 cm^2.

$$CR_{D3} \cong 2\pi A_0 \, f(E{>}100 \text{ MeV}) = 2\pi \, (1.50 \text{ cm}^2) \, (14.7 \times 10^3 \text{ p-cm}^{-2}\text{-sec}^{-1}) / (4\pi \text{ sr})$$

$$= 11,025 \text{ sec}^{-1}$$

D4 Detector:

D4 is shielded by the rear plug ($E_{th} = 100$ MeV) on the back side and by S2 and the side Cu shielding on the front side. The front side shielding is thick enough to stop 100 MeV protons. The detector is 3.0 cm^2 in area.

$$CR_{D4} \cong 2\pi A_0 \, f(E{>}100 \text{ MeV}) = 2\pi \, (3.00 \text{ cm}^2) \, (14.7 \times 10^3 \text{ p-cm}^{-2}\text{-sec}^{-1}) / (4\pi \text{ sr})$$

$$= 22,050 \text{ sec}^{-1}$$

12

3.3.2. Scintillators (S1, S2 and S3)

The three scintillators have a surface area in the shape of a right circular cylinder. The flux through such a surface can be accurately estimated as follows:

1) Consider a rectangular box, with a square cross section, circumscribed about the cylinder.

2) The count rate of particles through the box, CR_{BOX}, is

$$CR_{BOX} = f(E) \sum_{i=1}^{6} \pi A_i \tag{5}$$

where A_i is the area of the ith side. Note that the single hemisphere GF (πA_o) for each side is used in the calculation. This is to avoid double counting of particles incident on the box. Particles incident from the hemisphere below a given side will strike one of the other five sides first. Thus, using the two hemisphere GF will double count the particles traversing the box because each particle will be counted both when it enters and exits the box.

3) If the cylinder has a radius r and length h, the particle counting rate into the box will be

$$CR_{BOX} = \pi f(E) [8 (r^2 + rh)] \tag{6}$$

where the term in the brackets is the surface area of the box.

4) The actual surface area of the cylinder is $2\pi (r^2 + rh)$.

5) Approximate the cylinder counting rate by CR_{BOX}, multiplied by the ratio of the surface areas

$$CR_{CYL} = (2\pi / 8) CR_{BOX} = 0.78\pi f(E) [8 (r^2 + rh)] = 1.56 F(E) (r^2 + rh)$$

S1 Scintillator:

S1 has its front face shielded by the front collimator (E_{th} = 100 MeV), the back face by S2 (E_{th} = 120 MeV) and the bulk of its body by side Cu shielding (E_{th} = 60 MeV). A small section, underneath the light guide, will be shielded by the light guide itself ($E_{th} \cong$ 40 MeV) and by the Al housing over the PMT's. Overall, assume that protons with energies above 60 MeV will penetrate to S1 from all directions. The S1 radius, r, is 0.75 cm and the length, h, is 2.0 cm.

$$CR_{S1} \cong 1.56 (22.9 \times 10^3) (0.75^2 + 0.75 \times 2.0) = 74,000 \text{ sec}^{-1}$$

S2 Scintillator:

S2 has its front face shielded by S1 (E_{th} = 120 MeV), the back face by the rear plug (E_{th} = 100 MeV) and the bulk of its body by side Cu shielding (E_{th} = 60 MeV). A small section, underneath the light guide, will be shielded by the light guide itself ($E_{th} \cong$ 40 MeV) and by the Al housing over the PMT's. Overall, assume that protons with energies above 60 MeV will penetrate to S2 from all directions. The S1 radius, r, is 1.0 cm and the length, h, is 2.0 cm.

$$CR_{S2} \cong 1.56 (22.9 \times 10^3) (1.0^2 + 1.0 \times 2.0) = 107,000 \text{ sec}^{-1}$$

13

S3 Scintillator:

The S3 scintillator is an annular detector, it does not have front and rear faces. The effect of this geometry is to remove the r^2 term from the brackets on the RHS of eq. (7). S3 is shielded by the side Cu shielding ($E_{th} = 60$ MeV). The S3 radius is 1.25 cm and its length is 2.0 cm.

$$CR_{S3} \cong 1.56 \, (22.9 \times 10^3) \, (1.25 \times 2.0) = 89{,}000 \text{ sec}^{-1}$$

3.4. False Coincidence Event Rates

The event rates for in-aperture protons must be compared to "false coincidence" events. In this type of event, two or more penetrating protons strike the HEP detectors in such a way as to be misidentified as a single high energy proton. Ideally, the false coincidence rate should be negligible compared to the true event rate. In cases where this condition is not true, true event count rates and spectra may still be recovered from the data if 1) the false event rate is not significantly greater than the true event rate, and 2) there is a technique to subtract the false events from the measured count rate and energy spectra.

The penetrating protons are randomly distributed in time. The distribution of time intervals between the arrivals of successive particles follows a Poisson distribution with the mean equal to the inverse of the incidence rate. Under this condition, if the coincidence resolution time is τ, then the false coincidence rate between m detectors, C_f, is given by

$$C_f = m \, n_1 \, n_2 \, ... \, n_m \, \tau^{(m-1)} \tag{8}$$

where n_i is the singles counting rate for the ith detector. In the case of two detectors,

$$C_f = 2 \, n_1 n_2 \tau \, . \tag{9}$$

In the subsequent analysis, it will be assumed that the coincidence resolution time, τ, is 100 ns. The various false coincidence events are summarized in Table 4 at the end of Section 3.4.

3.4.1. Type A Events

In this event type D1, D2 and S1 fire and D3, S2, D4 and S3 do not. Expected true event rate is 49 sec^{-1}. Initially, neglect the anti-coincidence shield S3 and consider only a D1· D2· S1 event. Since D1 and D2 are located close together, assume that if a particle strikes one of them it will also strike the other one. In this case, the random false event rate, FR_A, is

$$FR_{A1} = 2 \, (74{,}000 \text{ sec}^{-1}) \, (2{,}000 \text{ sec}^{-1}) \, (100 \times 10^{-9} \text{ sec}) = 30 \text{ sec}^{-1}.$$

However, this is not the only way a false Type A event may be recorded. Out-of-aperture protons, from the full 4π solid angle, with energies sufficient to penetrate the shielding, may cause true coincidences as they traverse D1, D2 and S1 on an oblique path. The solid angle for such events is defined by D1 and the front face of S1. The opening half-angle is about 50°. Using eq. (3) to compute the geometric factor from one hemisphere yields

$$GF_{D1S1} = \pi \, (0.25 \text{ cm}^2) \, (1 - \cos^2(48°)) = 0.43 \text{ cm}^2\text{-sr}.$$

14

Since D1 is shielded by the front collimator ($E_{th} = 100$ MeV) on one side and by S1 and the Cu shielding ($E_{th} = 60$ MeV) on the other, the expected false event rate will be

$$FR_{A2} = GF_{D1S1} * [f (E > 100 \text{ MeV}) + f (E > 60 \text{ MeV})] = 1,290 \text{ sec}^{-1} .$$

It is clear that the false event rate is much greater than the true event rate and that the anti-coincidence shield S3 will be necessary if useful data on protons with energies below 120 MeV are to be obtained. A veto efficiency of about 95% will be needed in order to reduce the false event rate to the level of the true event rate.

The true event energy spectrum can be obtained from the measured energy spectrum by subtracting the false event energy spectrum (multiplied by a scaling factor which depends on the D1 and S1 singles rates and on the measured veto efficiency). The energy spectrum of the false coincidence events may be obtained by recording the energy spectrum of D1· D2· S1· S3 events.

<u>False Veto</u>

Another problem event is the false veto. In this case, there is valid Type A event and a random count occurs in any one of the other detectors, thus giving the signature of a bad event. The false veto rate, FV_A, is to a good approximation the sum of the coincidence rates of valid Type A events, CR_A, and the singles rates in the other HEP detectors

$$
\begin{aligned}
FV_A \quad &= 2 \, CR_A \, (CR_{D12} + CR_{D3} + CR_{D4} + CR_{S2} + CR_{S3}) \, \tau \\
&= 2 \, (50 \text{ sec}^{-1}) \, (2,000 + 11,025 + 22,050 + 107,000 + 89,000 \text{ sec}^{-1}) \, (100 \times 10^{-9} \text{ sec}) \\
&= 2.3 \text{ sec}^{-1}
\end{aligned}
$$

This rate is only about 5% of the true event rate.

3.4.2. Type B Events

In this event type D1, D2, S1, D3 and S2 fire and D4 and S3 do not. Expected true event rate is 4.5 sec^{-1}. The most likely false event scenario is the simultaneous passage of two particles, one through D1, D2 and, possibly, S1 and the second one through D3 and, possibly S1 and/or S2. This event rate is given by

$$
\begin{aligned}
FR_B \quad &= 2 \, CR_{D12} \, CR_{D3} \, \tau \\
&= 2 \, (2,000 \text{ sec}^{-1}) \, (11,025 \text{ sec}^{-1}) \, (100 \times 10^{-9} \text{ sec}) \\
&= 4.4 \text{ sec}^{-1}
\end{aligned}
$$

Note that this calculation neglects S3 which will veto out many of these false coincidences.
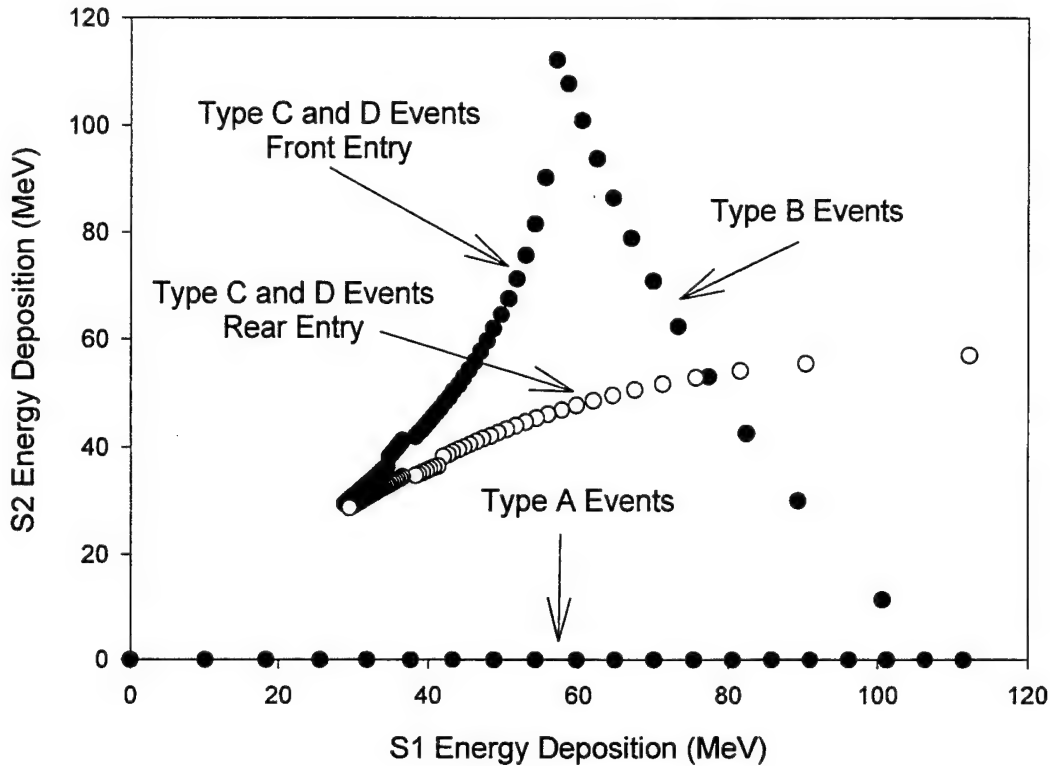
Figure 5. S1-S2 plane view of proton energy deposition in S1 and S2.

An additional discrimination against this type of false event will be provided by the pulse height analysis. The allowed range of S1 and S2 pulse heights for type B events is very restricted (see Figure 5) falling along an almost straight line in the S1-S2 plane, in particular S1 > 60 MeV. The pulse height distribution of the false coincidence event is expected to be very different. For example, out-of-aperture particles which hit S1, D3 and S2 will travel through very oblique paths through the instrument, thus keeping their paths in S1 and S2 short. This will result in relatively small energy deposition in S1 and S2, which will place the event in the lower left hand quadrant of the plot in Figure 5 and mark the event as invalid. (In Figure 5, the first data point (0,0) represents energy deposition by 15 MeV protons, each subsequent point is in 5 MeV increment. Data points go left to right for Type A events, up the Type B event line and down the Type C and D event lines. Open circles are for rear entry protons.).

The use of S3 and pulse height analysis should reduce the false coincidence rate to well below the expected true rate of 4.5 sec^{-1} and background spectrum subtraction from the measured energy spectrum should not be necessary. If the background must be subtracted, the true event energy spectrum can be obtained from the measured spectrum by subtracting the false event energy spectrum (multiplied by a scaling factor which depends on the D1 and D3 singles rates and on the measured S3 and pulse height analysis veto efficiency). The energy spectrum of the false coincidence events may be obtained by a suitable combination of the S1 and S2 energy spectra of events with a D1 or D2 singles trigger and events with a D3 singles trigger.

<u>False Veto</u>

There are two possible false vetoes for type B events, random S3 and/or D4 counts. Note that the effect of the second veto is not to get rid of the event but to erroneously identify it as a Type C or D event. The false veto rate is

$$FV_B = 2\, CR_B\, (CR_{D4} + CR_{S3})\, \tau$$

$$= 2\, (4.5\ \text{sec}^{-1})\, (22{,}050 + 89{,}000\ \text{sec}^{-1})\, (100 \times 10^{-9}\ \text{sec})$$

$$= 0.1\ \text{sec}^{-1}$$

3.4.3. Type C and D Events

In this event type D1, D2, S1, D3, S2 and D4 fire and S3 does not. Expected true event rate is 9.1 sec^{-1} for C type and 3.5 sec^{-1} for D type events. Several different types of false coincidence events will be considered.

<u>Event C1: Random triple coincidence</u>

Three independent particles strike D1and D2, D3 and D4 simultaneously. The event rate is

$$FR_{C1} = 3\, CR_{D12}\, CR_{D3}\, CR_{D4}\, \tau^2$$

$$= 3\, (2{,}000\ \text{sec}^{-1})\, (11{,}025\ \text{sec}^{-1})\, (22{,}050\ \text{sec}^{-1})\, (100 \times 10^{-9}\ \text{sec})^2$$

$$= 0.015\ \text{sec}^{-1}$$

<u>Event C2: Valid or false Type A event in coincidence with rear entry proton</u>

A valid or false Type A event (see Section 3.4.1) occurs in random coincidence with a rear entry proton which strikes D4, S2 and D3. The solid angle subtended by D3 and D4 is 0.43 cm^2-sr and the minimum energy needed to penetrate the rear shield and the S2 scintillator is abut 160 MeV so that

$$CR_{D34} = GF * f\,(E > 160\ \text{MeV}) = (0.43\ \text{cm}^2\text{-sr})\, (8.6 \times 10^3\ \text{p-cm}^{-2}\text{-sec}^{-1})\, /\, (4\pi)$$

$$= 295$$

The C2 event rate is

$$FV_{C2} = 2\, FR_{A2}\, CR_{D34}\, \tau$$

$$= 2\, (1{,}290\ \text{sec}^{-1})\, (295\ \text{sec}^{-1})\, (100 \times 10^{-9}\ \text{sec})$$

$$= 0.08\ \text{sec}^{-1}$$

Note that the allowed S1 and S2 pulse heights fall in a small section of the S1-S2 plane (see Figure 5). Most of the C2 events will fall outside the allowed range, thus permitting additional discrimination against these events.

<u>Event C3: Valid or false Type B event in coincidence with rear entry proton</u>

A valid or false Type B event (see Section 3.4.2) occurs in random coincidence with a rear entry proton which strikes D4 and S2. The event rate is

$$FV_{C2} = 2 (CR_B + FR_B) CR_{D4} \tau$$

$$= 2 (4.5 + 4.4 \text{ sec}^{-1}) (22,050 \text{ sec}^{-1}) (100 \times 10^{-9} \text{ sec})$$

$$= 0.04 \text{ sec}^{-1}$$

It appears the false coincidence rate of type C and D events will be small compared to the true rate, thus allowing a determination of the flux of high energy protons without any background subtraction. The main difficulty with these events will be the reconstruction of the original incident proton energy.

3.4.4. Electron Induced Events

The Al absorber in the HEP aperture is 0.127 cm thick, corresponding to the range of 700 keV electrons. The maximum steady state, radiation belt electron integral flux above 700 keV is about 6×10^6 e/cm^2-sec. This corresponds to an in-aperture count rate of

$$CR_e = GF * [f (E > 0.7 \text{ MeV})$$

$$= (11.7 \times 10^{-3} \text{ cm}^2\text{-sr}) (6.0 \times 10^6 \text{ p-cm}^{-2}\text{-sec}^{-1}) / (4\pi \text{ sr})$$

$$= 5,600 \text{ sec}^{-1}$$

Table 4. Listing of HEP false coincidence events.

Type	Designation	Description
A	FR_{A1}	Two protons hit D1, D2 and S1
A	FR_{A2}	Out-of-aperture single proton hits D1, D2 and S1
Veto A	FV_A	Valid Type A in coinc. with any other detector (false veto)
B	FR_B	Two or more protons, hit D1, D2 and D3 (also S1 and S2)
Veto B	FV_B	Valid Type B in coinc. with any other detector (false veto)
C	FR_{C1}	Random triple coinc. (D1&D2, D3 and D4)
C	FR_{C2}	Valid or False Type A event in coinc. with rear entry proton
C	FR_{C3}	Valid or False Type B event in coinc. with rear entry proton

The energy losses of energetic electrons are of the order of 270 keV in the solid state D1 and D2 detectors, so that the high threshold energy of 250 to 300 keV should strongly discriminate against the detection of electrons. Thus, the inner belt electrons should pose no difficulty for HEP. Under extreme conditions, following major solar events, this rate could increase by several orders of magnitude at altitudes above L = 1.7 R_E. There may be conditions under which the accurate measurement of high energy protons in the slot region and the outer belt is not possible because the electron event rate will be excessively high.

The Cu shielding surrounding the instrument is sufficient to stop 7 MeV electrons. Under normal conditions, the fluxes of these electrons are low (much less than 100 e/cm^2-sec) and will not cause any difficulty. Under extreme conditions, following major solar events, the flux of high energy electrons may increase sufficiently to cause measurement difficulties. However, this can only occur in the slot and outer belt regions and not in the inner belt.

3.5. Electronic Design

The over all HEP signal processing scheme is as follows (see Figure 6). The event trigger is formed when pulses in D1 and D2, and possibly D3, D4 and S3 exceed a fast discriminator threshold, set to about 250 keV of energy deposition (4 MeV for S3). The firing status of these detectors is converted to a five bit pattern, where each detector is represented by one bit (1-detector fired, 0-did not fire). Of the 32 possible bit patterns only 3 correspond to valid Type A, B, C and D events. Other bit patterns represent "bad" events although some of them may need to be measured in order to determine the energy spectra and count rates needed for background subtraction. The Coincidence Register, CR, (time resolution: 100 ns) determines if the event bit pattern matches one of the acceptable ones (there would be 6 acceptable patterns, the choice of which patterns are acceptable would be under the control of the DPU). If the event bit pattern does not match an acceptable pattern, no further processing is done. If an acceptable match is found, the Coincidence Register signals the Event Trigger Unit (ETU) which in turn 1) sends gates to the S1 and S2 ADC's, turning them on, and 2) sends a signal to the Local Event Processing Logic (LEPL) circuitry. LEPL performs a fast analysis on 1) the D1-D4 pulse heights (using the outputs of the quad discriminators) and 2) the CR bit pattern and computes the event ID word. The event ID is sent to the Local Lookup Table and Data Storage (LLTDS) where it controls how the digitized pulse heights from S1 and S2 are stored. Every 5-10 seconds, the DPU signals the LLTDS and the scaler (which counts events in each of the seven detectors) to send the accumulated data, which is further analyzed by the DPU and prepared for transmission to the spacecraft.

The current scope of the Amptek, Inc. SOBEDS effort does not include the DPU. The DPU functions discussed above are for a "generic" DPU.
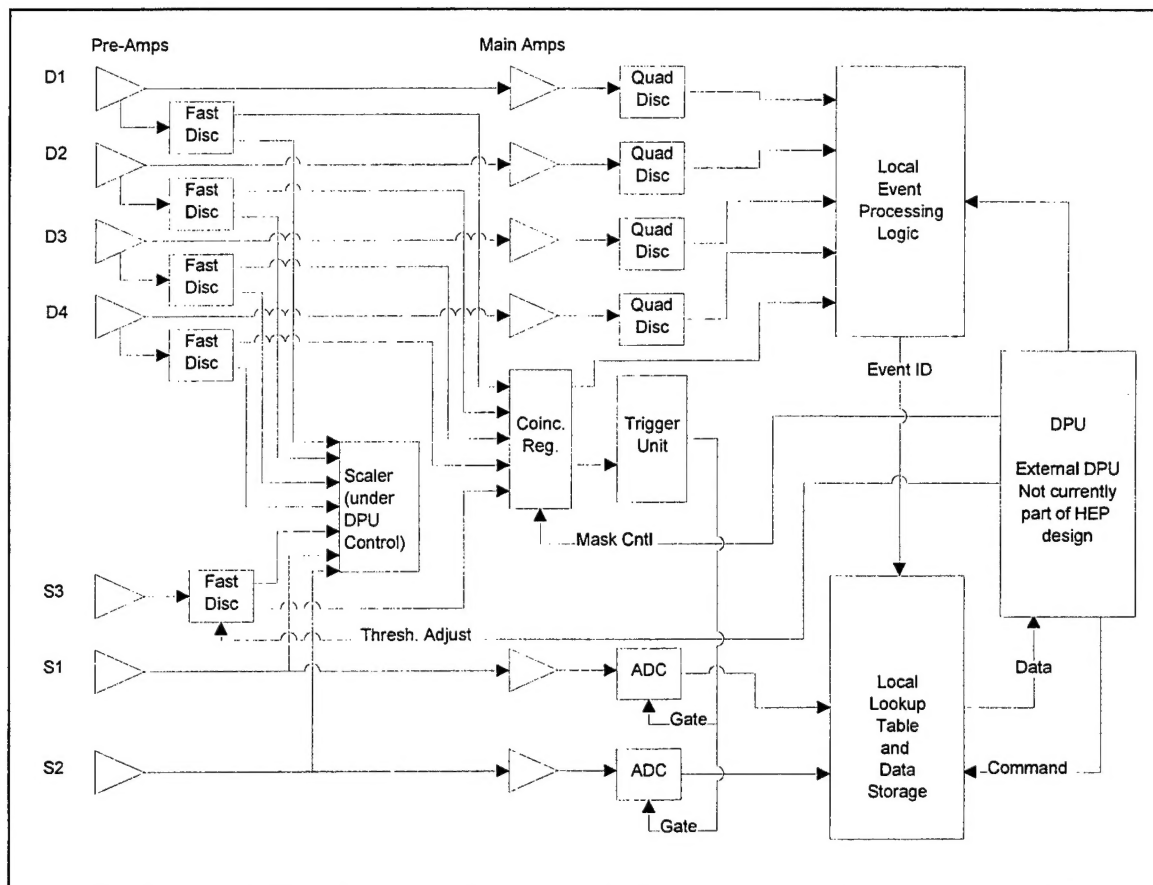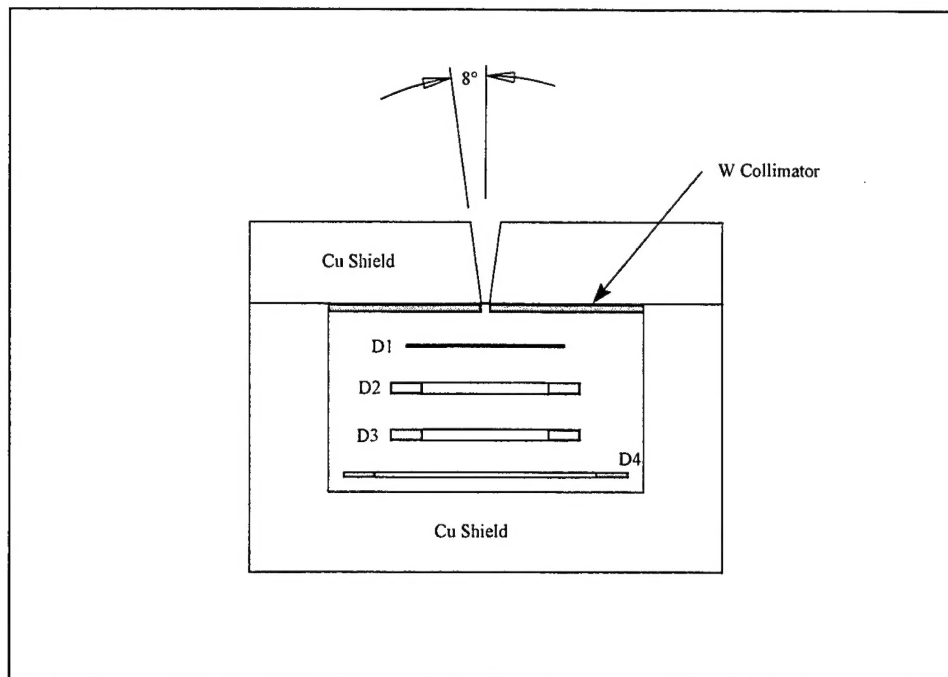
Figure 6. Block diagram of HEP electronics.

Figure 7. Schematic cross section diagram of the LEP sensor head.

4. BASELINE LEP INSTRUMENT DESIGN

The Low Energy Particle (LEP) instrument is intended to measure differential fluxes of protons with energies between 1 and 15 MeV and electrons with energies between 0.1 and 1 MeV. LEP sensor head consists of four Si solid state detectors in a telescope configuration (see Figure 7). The Cu shielding will be approximately 0.5 cm thick, enough to stop 60 MeV protons and 7 MeV electrons. The Al foil at the entrance aperture will be 0.009 cm thick, preventing protons with energies below 800 keV and electrons with energies below 30 keV from reaching the D1 detector.

The upper part of the LEP proton energy range will overlap with the lower part of the HEP instrument range. This will allow on-orbit cross-calibration between these two instruments. It may also be possible to cross-calibrate LEP with the DOS instrument, although there are significant difficulties with comparing data between dosimeter and telescope type instruments.

Electrons and protons are differentiated from each other, and their incident energy is determined by the pattern of energy loss in the Si detectors. Proton energy losses in Si detectors can be accurately calculated using analytic expressions and measured proton energy loss data (for example Janni's tables, AFWL-TR-65-150). The calculated energy losses of energetic protons in the LEP detectors are shown in Figure 8. Protons with energies above 15 MeV punch through the D3 and induce a signal in the D4 veto detector.
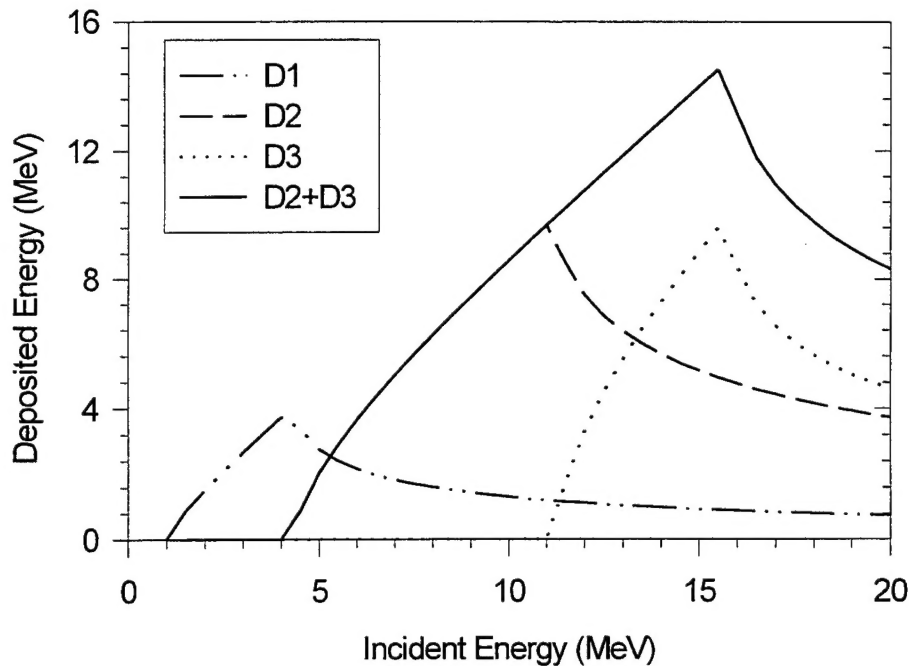
Figure 8. Calculated proton energy loss in LEP detectors.

Electron energy losses in LEP detectors cannot be calculated so simply because of the large amount of scattering that electrons suffer when traversing matter. We have undertaken a series of Monte Carlo calculations (Integrated Tiger Series code) of the electron energy losses in the LEP detectors. These calculations are being done in collaboration with our consultant, Dr. Stanley Woolf of Arcon Corp.

We are also undertaking a more sophisticated calculation of proton energy losses in the LEP detectors for the same geometry as the ITS electron calculations. The results of these calculations will be used to further refine the LEP design. A key aspect of these calculations will be to determine how different sizes of the detector impact the efficiency and energy resolution of the electron and higher energy proton measurements.

A series of electron (0.03 to 1.8 MeV) and proton (0.8 to 1.8 MeV) particle beam measurements with a prototype LEP sensor head was carried out at GSFC in April 1996. The results of this beam work were used to validate the LEP response calculations and test the performance of the sensors. The results of the data analysis showed that the measured and calculated LEP responses were in good agreement and that the sensor performance was satisfactory.

5. SUMMARY AND CONCLUSIONS

The outcome of the work performed during the first year of the contract has resulted in the baseline designs for both the SOBEDS HEP and LEP sensors. The HEP sensor engineering model is currently being manufactured for testing with proton beams. The physical construction of the LEP sensor has been deferred as a result of PL request.

The HEP design has been optimized for operation in the inner radiation belt. The configuration of the detectors has been arranged to permit a clean measurement of in-aperture protons with energies between 15 and 300 MeV in the presence of an intense flux of high energy protons. This type of measurement requires the use of fast, multiple detector coincidence logic and an anti-coincidence scintillator shield. The HEP engineering model, which embodies the baseline design will be built and tested during the second year of the SOBEDS contract. The planned work on the HEP engineering model will include proton beam experiments at the Harvard Cyclotron (30 < E < 150 MeV) and the Brookhaven National Laboratory Alternating Gradient Synchrotron (E> 125 MeV).

The LEP baseline design has been investigated using computer simulation methods. The instrument design is sufficiently straightforward, so that we have high confidence in the accuracy of the computed results. Once we are directed by PL to build this sensor, we will proceed rapidly to the manufacture of the LEP engineering model and perform the necessary electron and proton beam calibrations.